Analysis of Human Peripapillary Atrophy Using Computerised Image Analysis

Ştefan Ţălu[1], Zoltán Fazekas[2], Mihai Ţălu[3] and Stefano Giovanzana[4]

[1] Technical University of Cluj-Napoca, Faculty of Mechanics, Department of AET, Discipline of Descriptive Geometry and Engineering Graphics, Cluj-Napoca 400641, Romania
Email: stefan_ta@yahoo.com

[2] Systems and Control Laboratory, Computer and Automation Research Institute, Budapest, Hungary
Email: fazekas.zoltan@sztaki.mta.hu

[3] University of Craiova, Faculty of Mechanics, Department of Applied Mechanics, Craiova 200585, Romania
Email: mihai_talu@yahoo.com

[4] University of Milan-Bicocca, Milano, 20126, Italy
Email: lol_740@hotmail.com

Abstract. Retinal morphological changes around the optic disc are looked at in the paper; more specifically the vascular network geometry in healthy patients and patients with peripapillary atrophy are quantified and compared using a multifractal approach. Segmented and skeletonized retinal images from the DRIVE database were analyzed. Multifractal and lacunarity analyses of the binary images were carried out using the Image J software. It was found that the vascular network geometry in patients with peripapillary atrophy has a multifractal geometry characterized by a hierarchy of exponents.

Keywords: Multifractals, Lacunarity, Retina, Microvasculature, Peripapillary atrophy.

1 Introduction

1.1 Optic disc

The optic disc – or optic nerve head (ONH) – is one of the distinctive anatomical features that are usually visible in a fundus image of the human retina. The ONH is the entrance of the blood vessels and of the optic nerve into the retina. The central retinal artery and central retinal vein emanate through the bundles of optic nerve. The mentioned central retinal blood vessels carry the blood for the upper layers of the retina, while the optic nerve serves as the conduit of information flow from the eye to the brain. The ONH appears as a circular area, usually as a bright yellow or white region, with a diameter of roughly one-sixth of fundus image's diameter. It is

perceivably brighter than the surrounding retinal area, and appears as the convergent area of the blood vessel vascular network.

The identification of the ONH is an important processing step in the detection and the analysis of retinal structures, and – in case of pathologies – the problematic or unusual retinal features. In case of healthy retinas, all the aforementioned properties (i.e., shape, colour, size, blood vessel convergence) aid the identification of ONH's, while in case of pathologies, only a subset of these properties can be used for the purpose. As mentioned above, the ONH's usually appear as circular areas in the fundus images, however, in some snapshots, they are better approximated with ellipses. The latter case is due to the non-zero angle between image plane and the plane of the optic disc. See various ONH examples, geometric models and locating methods in [1], [2], [3] and [4].

1.2 Peripapillary atrophy

Peripapillary atrophy (PPA) refers to a white or pigmented crescent-shaped area adjacent to the ONH. The atrophy may be confined to a small area adjacent to the ONH. The area in this case appears mostly either in the temporal or in the lower temporal direction from ONH. The atrophy can also be extensive; in this case it fully surrounds the ONH. Based on the extent of the tissue atrophy, the PPA can be categorized into two stages and the corresponding retinal regions are referred as zones α and β, respectively. Zone α is the region with pigmentary and structural irregularity of retinal pigment epithelial cells (RPE cells). Zone β corresponds to region with complete loss of the RPE cells accompanied by variable loss of the photo-receptors [5] and [6].

1.3 Digital imaging in ophthalmology

Throughout the last three decades, consecutive generations of retinal cameras and digital imaging systems have offered higher and higher resolutions in respect of fundi. The advantage of digital imaging is markedly perceptible in retinal imagery and in ophthalmic imagery in general. The obtained ophthalmic images are unswervingly available for quantitative analysis, which is achieved by simple or more complex mathematical manipulations of the image data (e.g., fundus image data), even for long periods of time. As a consequence, ophthalmic image archives can be set up for individual patients and their ophthalmic medical history can be traced in their respective images.

The fundus images used herein as examples are taken from the Digital Retinal Images for Vessel Extraction (DRIVE) database, which itself is a special purpose research database and does not contain individual medical histories, but as such it also illustrates the point made above. The DRIVE database was originally set up to facilitate comparative studies on segmentation of blood vessels in retinal images, [30] and [31].

1.4 Fractal-like morphology of the retinal vascular network

The morphogenesis of the human retinal vascular network can be considered as a diffusion-limited aggregation process [10]. Such processes may result in branching networks. These morphologically very similar branching networks appear in nature in seemingly unrelated areas; in areas studied by different disciplines [35].

The resulting branching networks – including the human retinal vascular network – exhibit fractal-like structural characteristics, e.g., the self-similarity at low resolutions, see [7], [8], [9] and [10]. In case of the human retinal vascular network, these structural characteristics can be observed *in vivo* using a retinal camera.

Fractal and multifractal analyses have been widely used in the medical assessment of the optic fundi, see e.g., [11], [12], [18], [21] and [22]. These mathematical analyses offer a *natural* description of the retinal vessel structure and morphology, see [14], [15], [16], [17], and are utterly useful in detection, description and diagnosis of various vascular and non-vascular pathological symptoms and cases, see e.g., [13], [19], [20] and [25].

According to investigations reported in the literature, the fractal dimension of the vascular network present in a healthy human retina is approximately 1.7, see [7], [10]. However, there is no consensus in the literature concerning the fractal dimensions of the vascular networks in human retinas affected by particular pathological disorders, see e.g., [7], [19], [21] and [25] in this respect.

In another study, the human retinal vascular network was found to have a multifractal geometrical structure [21]. Fractal and multifractal analysis of retinal vascular network pattern and geometry is considered a useful screening tool to assess the bifurcation geometry and vessel pattern complexity for quantifying and detecting retinal vascular diseases.

2 Materials and methods

2.1 Multifractal analysis

In our study, the method defined by Chhabra and Jensen was used for the direct computation of the multifractal spectrum [26]. The generalized dimension D_q with its real parameter q, where $q \neq 1$ and $-\infty < q < +\infty$ and where q's negative values correspond to and characterize the sparse regions of the structure to be evaluated and q's positive values correspond to the dense regions, is defined as follows.

$$D_q = \frac{1}{q-1} \lim_{\varepsilon \to 0} \frac{\ln Z(q,\varepsilon)}{\ln \varepsilon} \tag{1}$$

The partition function $Z(q, \varepsilon)$ furnishes information – at different scales and using moments of different orders – about the structure to be evaluated, i.e., in our case, about the network of retinal blood vessels. The scale is represented by ε, which is the size of the boxes used for covering the structure, and the moments are computed at

order q. To fill the missing D_q value at $q = 1$, D_1 is defined as limit of D_q as q approaches to 1. Generalized dimensions D_0, D_1, and D_2 are known as the capacity dimension, information dimension and correlation dimension, respectively. They satisfy the following inequality: $D_0 \geq D_1 \geq D_2$. The limits of the generalized dimension spectrum as q approaches negative infinity and positive infinity, respectively, are $D_{-\infty}$ and D_{∞}, see [16], [21] and [26].

Methods are available from the literature for computing various multifractal spectra, see e.g., [27]. Apart from the mentioned generalized dimension spectrum *D(q),* i.e., D_q as function *of q,* also the *f(α)* spectrum is frequently used in multifractal analysis. α is the Hörder-, or singularity exponent, which is the local degree of singularity.

For a fractal, its generalized dimension spectrum *D(q)* is constant for all *q*'s, while for a multifractal, *D(q)* is a monotone decreasing function. The relationship between *D(q)* and *f(α)* is as follows.

$$f(\alpha(q)) = q\alpha(q) - \tau(q) \tag{2}$$

where *α(q)* represents the Hölder-exponent of the *q*-th order moment and can be expressed as follows:

$$\alpha(q) = \frac{d\tau(q)}{dq} \ . \tag{3}$$

In the above equations, *τ(q)* is the mass correlation exponent of the corresponding generalized dimension spectrum *D(q)* and it is defined as

$$\tau(q) = (q-1)D_q \ . \tag{4}$$

Another useful measure used for the characterization of fractal and multifractal structures is lacunarity. It is a measure of the structural heterogeneity in the structure [28]. It is a measure of how the fractal object fills the space. The use of lacunarity allows the determination of gaps in the pattern.

2.2 Images used in the evaluation

Four retinal images and their segmented and skeletonised versions were selected and used from the training images of the aforementioned image database. Two out of the four retinal images were taken of healthy retinas. The remaining two images were taken of retinas with pathology, namely peripapillary atrophy. The images were JPEG-compressed. The little bulge on the image-disk at 45° is ensures the proper orientation of the image and prevents accidental mixing up the images of the right and the left eyes.

In Figs. 1 and 2, two fundus images are shown – together with their corresponding segmented and skeletonised versions – out of the considered four. Normal fundus of a right eye is shown in Fig.1; while in Fig. 2, the fundus image of a left eye is presented. The retina appearing in the latter figure is affected by peripapillary atrophy.

The images were acquired using a Canon CR5 non-mydriatic 3CCD camera with a 45 degree field of view (FOV). Each image was captured using 8 bits per color plane at 768 by 584 pixels. The FOV of each image was circular with a diameter of approximately 540 pixels. The images are cropped around the FOV and a mask image is provided that delineates the FOV. Mask images are in gif format. The binary skeletons were directly extracted using the morphologic operations from the original micrograph images.

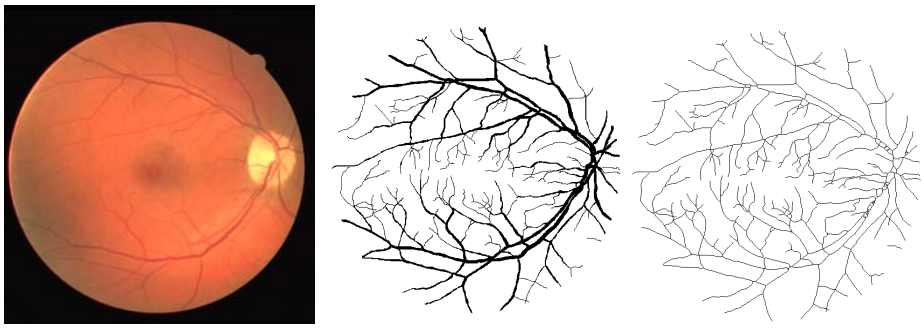

Fig. 1. Fundus image of a right eye with normal retinal blood vessel network (image `27_training.tif` from the DRIVE image database). From left to right: original color image, segmented image and its skeletonized version.

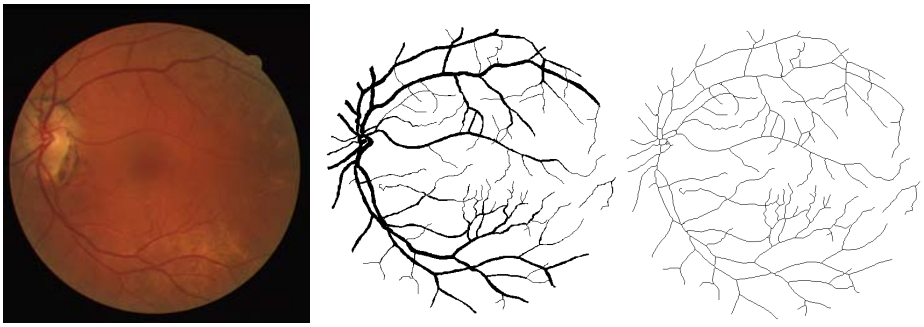

Fig. 2. Fundus image of a left eye (image `26_training.tif` from the DRIVE image database). Its retinal vessel network is affected by peripapillary atrophy. From left to right: original color image, segmented image and its skeletonized version.

3 Results

Fractal and multifractal analyses were performed – in respect of the segmented images and their skeletonized versions mentioned in Subsection 2.2 – using the Image J software [32] and the FracLac plug-in [33]. These analyses were based on the well-known box counting algorithm [38]. The central tendency and dispersion measure were expressed by the mean value and standard deviation.

The evaluation of the images was carried out with the following program settings. Four different starting positions of the grid were used in box counting stage for each box-size. The grid calibres were computed for scaled series. The standard multifractal data processing package was used in respect of the best sample gained. Full scan was carried out for each sample. The evaluation was carried out five times for each image with slightly different selections of the processed image area. The final D(q) values were calculated as the averages over these repetitions.

Table 1. The generalized dimensions (D_q) for q = 0, 1 and 2; and the mean lacunarity Λ found in the analyzed images of healthy retinas.

Image no.	Status	Type	D_0	D_1	D_2	Λ
27_…	normal	segm.	1.6913	1.6262	1.5895	0.5317
		skelet.	1.6755	1.6461	1.6241	0.2643
28_…	normal	segm.	1.7113	1.6160	1.5558	0.5402
		skelet.	1.6914	1.6616	1.6414	0.2368
Average	**normal**	**segm.**	**1.7013**	**1.6211**	**1.5726**	**0.5359**
		skelet.	**1.6834**	**1.6538**	**1.6327**	**0.2505**

Table 2. The generalized dimensions (D_q) for q = 0, 1 and 2; and the mean lacunarity Λ found in the analyzed images of retinas affected by peripapillary atrophy.

Image no.	Status	Type	D_0	D_1	D_2	Λ
26_…	pathol.	segm.	1.6571	1.5907	1.5642	0.5803
		skelet.	1.6319	1.6083	1.6014	0.2561
31_…	pathol.	segm.	1.5997	1.5318	1.4951	0.6235
		skelet.	1.5680	1.5382	1.5146	0.3054
Average	**pathol.**	**segm.**	**1.6284**	**1.5612**	**1.5296**	**0.6019**
		skelet.	**1.5999**	**1.5732**	**1.5580**	**0.2807**

The gaps in the vascular patterns were quantified by lacunarity values. The mean lacunarity Λ is computed by the Image J software as follows:

$$\Lambda = \left(\sum \left[1 + (\sigma / \mu)^2\right]\right) / n \ , \tag{5}$$

where σ is the standard deviation, μ is the mean of the number of object pixels found per box – in case of a particular box-size – during a box count at a given orientation, while n is the number of box sizes.

The multifractal and lacunarity results obtained for the mentioned fundus images are given in Table 1.

3.1 Statistical analysis

The statistical analysis of the multifractal results was accomplished using the GraphPad InStat software program [34]. The Kolmogorov-Smirnov test, for testing the normality of the distributions of generalized dimensions (D_q) and lacunarity parameter Λ, were performed for the healthy and the pathological retinas, as well. It has turned out that the generalized fractal dimensions of the vascular trees and the lacunarity parameters obtained from the image measurements described above followed normal distributions. Values with $p < 0.05$ were regarded statistically significant.

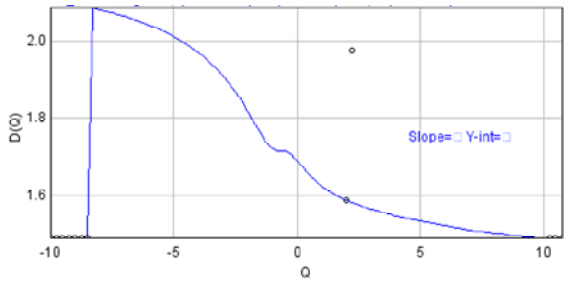

Fig. 3. The *D(q)* spectrum – obtained with Image J – of the vascular network of a healthy retina.

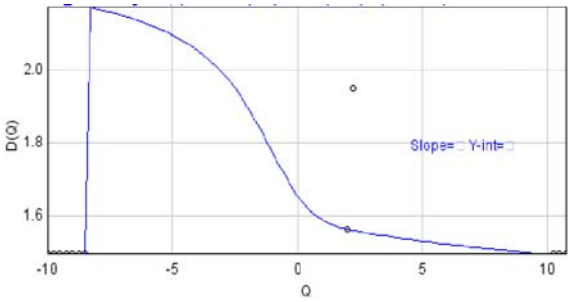

Fig. 4. The *D(q)* spectrum of the vascular network of a retina affected by peripapillary atrophy.

Table 1 show that the average of generalized dimensions D_0, D_1, and D_2 computed for the entire retinal areas imaged and characterizing the retinal networks are somewhat lower for the retinas affected by peripapillary atrophy than for normal retinas. This statement is true for the segmented and for the skeletonised images of the retinal vascular trees images alike.

Furthermore, it was also observed that the mean lacunarity Λ is slightly greater for the pathological retinas than for normal retinas. Again, this statement is true for both segmentation methods used. The measurement data in Table 1 show that skeletonisation of the segmented blood vessels slightly reduces the generalized dimensions and lacunarity values.

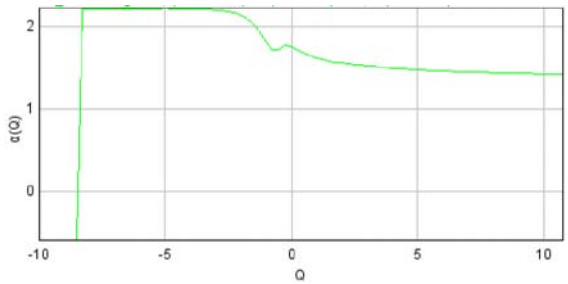

Fig. 5. The Hölder-exponent α *(q)* computed for the vascular network of a healthy retina.

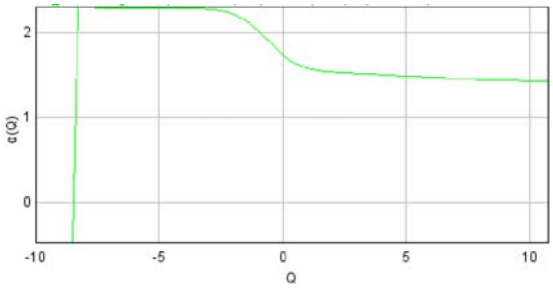

Fig. 6. The Hölder-exponent α *(q)* computed for the vascular network of a retina affected by peripapillary atrophy.

The results obtained from the multifractal and lacunarity analysis of image file `27_training.tif` – or more precisely from its manually segmented version `27_manual1.gif` – are plotted in Figs. 3, 5, and 7. The corresponding results computed for the manually segmented image file `26_manual1.gif` – obtained from image file `26_training.tif` – are plotted in Figs. 4, 6 and 8.

Comparing the diagrams in Figs. 3 and 4, one can identify two important changes: the higher value of $D(q)$ near $q = -8$ and the lack of buckle over range $-1 < q < 1$ (characterizing the pathological case).

Similar changes are apparent, if one compares the spectra plotted in Figs. 5 and 6 – showing the Hölder-exponent of healthy and pathological retinas, respectively – and the spectra plotted in Figs. 7 and 8, which show the $f(\alpha)$ spectra of the vascular tree of a healthy and a pathological retina, respectively.

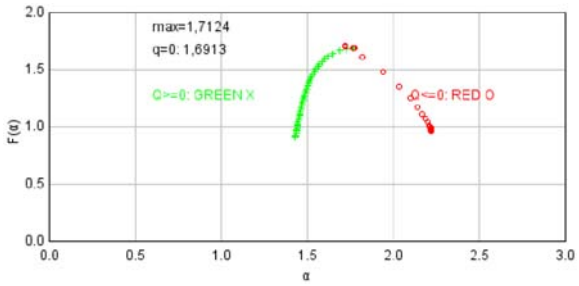

Fig. 7. The *f(α)* spectrum of the vascular network of a healthy retina.

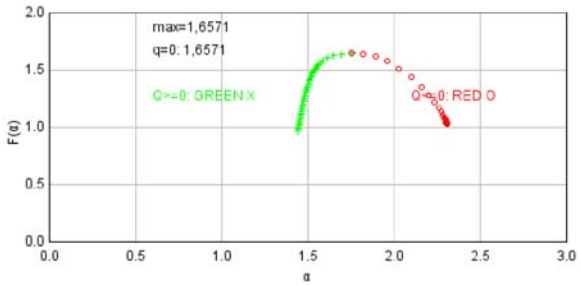

Fig. 8. The *f(α)* spectrum of the vascular network of a retina affected by peripapillary atrophy.

4 Discussion

As in case of retinal vascular morphogenesis, which was mentioned earlier in connection with the fractal-like structure of the retinal vascular tree, adequate oxygen levels and the adequate oxygen supply to the retina plays an important role in the proper functioning of the retina.

In vascularised retinas in general – and in human retinas in particular – oxygen is delivered to the retina via a combination of the choroidal vascular bed and the retinal vasculature. The high-oxygen demand of the retina and the relatively sparse retinal vasculature contribute to the particular vulnerability of the retina to vascular diseases.

A large proportion of retinal blindness is associated with diseases having a vascular component, and disrupted oxygen supply to the retina is likely to be a critical factor in these. Much attention has therefore been directed at determining the intraretinal oxygen environment in healthy and diseased eyes [39]. Our present small-scale experiment and analysis is also part of this interdisciplinary research effort.

In case of retinas affected by peripapillary atrophy, the reduction of the vascular tree affects unfavourably the nerve tissue. This reduction can be quantified using fractal and multifractal measures mentioned in the text. Considerable changes in particular values (e.g., D_0, D_1, and D_2) compared to the their normal ranges and easily detectable changes in the shape of spectra $D(q)$, $\alpha(q)$ and $f(\alpha)$ indicate the vascular loss. The presented small-scale experiment and analysis obviously should be seen as such. The found tendencies should be verified, measured and quantified in a more accurate manner in large-scale experiments and analyses.

5 Conclusion

Retinal morphological changes around the optic disc were looked at in the paper. More specifically the geometry of the vascular network found in healthy patients and patients with peripapillary atrophy were quantified and compared using a multifractal approach. For this purpose, segmented and skeletonised retinal images from the DRIVE database were analyzed.

The retinal vascular imaging offers the potential to provide information for quantifying the stage of peripapillary atrophy in human patients.

It was found that the vascular network geometry in patients with peripapillary atrophy has a multifractal geometry characterized by a hierarchy of exponents. Furthermore, significant changes – compared to the healthy cases – were identified in respect of generalised dimensions D_0, D_1, and D_2 and multifractal spectra $D(q)$, $\alpha(q)$ and $f(\alpha)$.

References

1. Walter, T., Klein, J. C.: Segmentation of color fundus images of the human retina: Detection of the optic disc and the vascular tree using morphological techniques. Medical Data Analysis, LNCS, vol. 2199, pp. 282--287, Springer-Verlag, Berlin (2001)
2. Hoover, A., Goldbaum, M.: Locating the optic nerve in a retinal image using the fuzzy convergence of the blood vessels, IEEE Trans Med Imaging, 22(8), pp. 951--958 (2003)
3. Youssif, A.R., Ghalwash, A. Z., Ghoneim, A. R.: Optic disc detection from normalized digital fundus images by means of a vessels' direction matched filter, IEEE Trans Med Imaging, 27(1): pp. 11-18 (2008)
4. Rangayyan, R. M., Zhu, X., Ayres, F. J., Ells A. L.: Detection of the optic nerve head in fundus images of the retina with Gabor filters and phase portrait analysis, J Digit Imaging. 23(4): pp. 438--453 (2010)
5. Manjunath, V., Shah, H., Fujimoto, J. G., Duker, J. S.: Analysis of peripapillary atrophy using spectral domain optical coherence tomography. Ophthalmology, 118(3): pp. 531--536., (2011)
6. Giaconi, J. A., Law, S. K., Coleman, A. L., Caprioli, J.: Pearls of glaucoma management, Springer-Verlag, Berlin, pp. 63--64 (2010)
7. Kyriacos, S., Nekka, F., Vicco, P., Cartilier, L.: The retinal vasculature: towards an understanding of the formation process. In Fractals in Engineering - From Theory to Industrial Applications, Vehel, L. J. Lutton, E., Tricot, G. (eds.), Springer-Verlag, Berlin, pp. 383--397 (1997)
8. Patton, N., Aslam, T. M., MacGillivray, T., Deary, I. J., Dhillon, B., Eikelboom, R. H., Yogesan, K., Constable, I. J.: Retinal image analysis: concepts, applications and potential, Prog. Retin. Eye Res., 25(1), pp. 99--127 (2006)
9. Family, F., Masters, B. R., Platt, D. E.: Fractal pattern formation in human retinal vessels, Physica D, 38, pp. 98--103 (1989)
10. Masters, B. R.: Fractal analysis of the vascular tree in the human retina, Annu. Rev. Biomed. Eng., 6 pp. 427--452 (2004)
11. Talu, S.: Mathematical models of human retina. Oftalmologia, 55(3), pp. 74--81 (2011)
12. Wainwright, A., Liew, G., Burlutsky, G., Rochtchina, E., Zhang, Y. P., Hsu, W., Lee, J. M., Wong, T. Y., Mitchell, P., Wang, J. J.: Effect of image quality, color, and format on

the measurement of retinal vascular fractal dimension. Invest. Ophthalmol. Vis. Sci., 51(11), pp. 5525--5529 (2010)
13. Doubal, F. N., Do retinal microvascular abnormalities shed light on the pathophysiology of lacunar stroke? PhD dissertation, University of Edinburgh, UK, (2010)
14. Jelinek, H., Mendonça, M. B., Oréfice, F., Garcia, C., Nogueira, R., Soares, J., Junior, R.: Fractal analysis of the normal human retinal vasculature. The Internet Journal of Ophthalmology and Visual Science, 8(2), pp. 1--4 (2010)
15. Talu, S.: Fractal analysis of normal retinal vascular network. Oftalmologia 55(4), pp. 11--16 (2011)
16. Talu, S.: Mathematical methods used in monofractal and multifractal analysis for the processing of biological and medical data and images. ABAH Bioflux 4(1), pp. 1--4 (2012)
17. Talu, S.: Texture analysis methods for the characterisation of biological and medical images. ELBA Bioflux, 4(1), pp. 8--12 (2012)
18. Azemin, M. Z., Kumar, D. K., Wong, T. Y., Kawasaki, R., Mitchell, P., Wang, J. J.: Robust methodology for fractal analysis of the retinal vasculature, IEEE Trans. Med. Imaging, 30(2), pp. 243--250 (2010)
19. Cheung, N., Donaghue, K. C., Liew, G., Rogers, S. L., Wang, J. J., Lim, S. W., Jenkins, A. J., Hsu, W., Li Lee, M., Wong, T. Y.: Quantitative assessment of early diabetic retinopathy using fractal analysis. Diabetes Care, 32(1), pp. 106--10 (2009)
20. Liew, G., Wang, J. J., Cheung, N., Zhang, Y. P., Hsu, W., Lee, M. L., Mitchell, P., Tikellis, G., Taylor, B., Wong, T. Y.: The retinal vasculature as a fractal: methodology, reliability and relationship to blood pressure. Ophthalmology, 115(11), pp. 1951--1956 (2008)
21. Stosic, T., Stosic, B.: Multifractal analysis of human retinal vessels, IEEE Trans. Med. Imaging, 25(8), pp. 1101--1107 (2006)
22. Talu, S., Giovanzana, S.: Fractal and multifractal analysis of human retinal vascular network: a review. HVM Bioflux, 3(3), pp. 205--212 (2011)
23. MacGillivray, T. J., Patton, N., Doubal, F. N., Graham, C., Wardlaw, J. M.: Fractal analysis of the retinal vascular network in fundus images. Proceedings of the International Conference of IEEE Engineering in Medicine and Biology Society, Lyon, France, pp. 6455--6458 (2007)
24. Mendonça, M. B., Amorim Garcia, C. A., Nogueira, R. A., Gomes, M. A., Valença, M. M., Oréfice, F.: Fractal analysis of retinal vascular tree: segmentation and estimation methods. Arq. Bras. Oftalmol., 70(3) pp. 413--422. (2007)
25. Lakshminanarayanan, V., Raghuram, A., Myerson, J. W., Varadharajan, S.: The fractal dimension in retinal pathology. J. Mod. Opt., 50(11), pp. 1701--3 (2003)
26. Chhabra, A., Jensen, R. V.: Direct determination of the f(α) singularity spectrum. Phys. Rev. Lett., 62, pp. 1327--1330 (1989)
27. Lopes, R., Betrouni, N.: Fractal and multifractal analysis: A review, Med. Image Anal., 13, pp. 634--649 (2009)
28. Allain, C., Cloitre, M.: Characterizing the lacunarity of random and deterministic fractal sets. Physical Review A, 44(6) pp. 3352--3558 (1991)
29. http://www.isi.uu.nl/Research/Databases/DRIVE/. Accessed 10 July 2012.
30. Niemeijer, M., Staal, J. J., van Ginneken, B., Loog, M., Abramoff, M. D.: Comparative study of retinal vessel segmentation methods on a new publicly available database. Proceedings of the International Symposium on Medical Imaging, San Diego, CA, USA, pp. 648--656 (2004)
31. Staal, J. J., Abramoff, M. D., Niemeijer, M., Viergever, M. A., van Ginneken, B.: Ridge-based vessel segmentation in color images of the retina, IEEE Trans. Med. Imaging 23(4) pp. 501--509 (2004)
32. http://imagej.nih.gov/ij. Accessed 10 October 2012.

33. http://rsbweb.nih.gov/ij/plugins/fraclac/FLHelp/Introduction.htm. Accessed 10 May 2012.
34. http://www.graphpad.com/instat/instat.htm. Accessed 10 October 2012.
35. Fazekas, Z.: Graph-based description of retinal blood-vessels in fluorescein angiograms. Proceedings of the 4th International Workshop on Systems, Signals and Image Processing, Poznan, Poland, pp. 235--238 (1997).
36. Fazekas, Z.: Shape description and image registration of ophthalmic images using 'Pierneef-trees'. Proceedings of PRASA 1999 (on CD), Weber, D. and Herbst, B. (eds), Stellenbosch, South Africa, pp. 1--6 (1999)
37. Posadas, A. N. D., Giménez, D., Bittelli, M., Vaz, C. M. P., Flury, M.: Multifractal characterization of soil particle-size distributions. Soil Sci. Soc. Am. J., 65, pp. 1361--1367 (2001)
38 Liebovitch, L. S., Toth, T.: A fast algorithm to determine fractal dimensions by box counting. Physics Letters A, 141(8–9), pp. 386--390, (1989)
39 Yu, D. Y, Cringle, S. J.: Oxygen distribution and consumption within the retina in vascularised and avascular retinas and in animal models of retinal disease. Progress in Retinal and Eye Research, 20(2), pp. 175--208 (2001)